Chapter 1

Sand Mold Press Casting with Metal Pressure Control System

Ryosuke Tasaki, Yoshiyuki Noda,
Kunihiro Hashimoto and Kazuhiko Terashima

Additional information is available at the end of the chapter

http://dx.doi.org/10.5772/51082

1. Introduction

A new casting method, called the press casting process, has been developed by our group in recent years. In this process, the ladle first pours molten metal into the lower (drag) mold. After pouring, the upper (cope) mold is lowered to press the metal into the cavity. This process has enabled us to enhance the production yield rate from 70% to over 95%, because a sprue cup and runner are not required in the casting plan [1]. In the casting process, molten metal must be precisely and quickly poured into the lower mold. Weight controls of the pouring process have been proposed in very interesting recent studies by Noda et al. [2]. However, in the pressing part of the casting process, casting defects can be caused by the pattern of pressing velocity. For example, the brake drum shown in Fig. 1 was produced with the press casting method. Since the molten metal was pressed at high speed, the product had a rough surface. This type of surface defect in which molten metal seeps through sand particles of the greensand mold and then solidifies, is called Metal Penetration. Metal penetration is most likely caused by the high pressure that molten metal generates, and it necessitates an additional step of surface finishing at the least. Thus, the product quality must be stabilized by the suppression of excess pressure in the high-speed press. For short-cycle-time of production, a high-speed pressing control that considers the fluid pressure in the mold is needed. Pressure control techniques have been proposed for different casting methods [3-4]. In the injection molding process, the pressure control problem has been successfully resolved by computer simulation analysis using optimization technique by Hu et al. [5] and Terashima et al. [6]. Furthermore, a model based on PID gain selection has been proposed for pressure control in the filling process. Although the pressure in the mold must be detected in order to control the process adequately using feedback control, it is difficult

to measure the fluid pressure, because the high temperature of the molten metal (T ≥ 1200 K) precludes the use of a pressure sensor. Thus, in our previous papers by Tasaki et al. [7], the pressure during pressing at a lower pressing velocity was estimated by using a simply constructed model of molten metal's pressure based on analytical results of CFD: Computational Fluid Dynamics. A new sequential pressing control, namely, a feed forward method using a novel simplified press model, has been reported by the authors of Ref. [7]. It has been shown that this method is very effective for adjusting pressure in the mold. However, in the previous paper, the actual unstationary flow and the temperature drop during pressing was not considered; a detailed analysis that considers the temperature change during pressing is required to reliably predict and control the process behaviors.

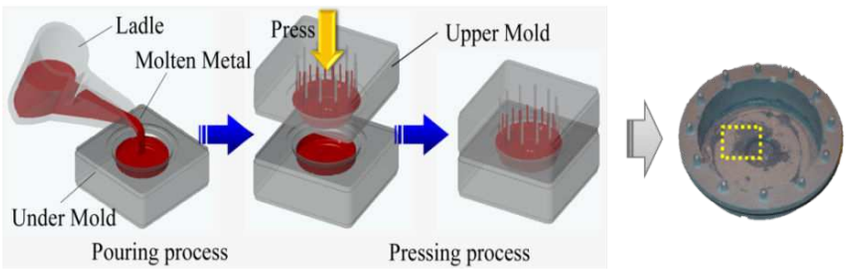

Figure 1. Pouring and pressing processes in press casting.

In this chapter, a novel mathematical model with the pressure loss term of fluid in vertical unstationary flow is derived by assuming that the incompressible viscous flow depends on the temperature drop of the molten metal. The model error for the real fluid's pressure is minimized by the use of parameter identification for the friction coefficient at the wall surface (the sole unknown parameter). Furthermore, the designed velocity of the switching pattern is sequentially calculated by using the maximum values of static, dynamic, and friction pressure, depending on the situation in each flow path during the press. An optimum design and a robust design of pressing velocity using a switching control are proposed for satisfying pressure constraint and shortening the operation time. As a final step in this study, we used CFD to check the control performance using control inputs of the obtained multistep pressing pattern without a trial-and-error process.

2. Pressing Process in Press Casting

The upper mold consists of a greensand mold and a molding box. The convex part of the upper mold has several passages that are called overflow area, as shown in Fig. 2. Molten metal that exceeds the product volume flows into the overflow areas during pressing. These areas are the only parts of the casting plan that provide the effect of head pressure. As the diagram shows, these are long and narrow channels. When fluid flows into such the area, high pressurization will cause a casting defect. Therefore, it is important to control the pressing velocity in order to suppress the rapid increase in pressure that occurs in high-speed

http://dx.doi.org/10.5772/51082

pressing. The upper mold moves up and down by means of a press cylinder and servomotor. The position of the upper mold can be continuously measured due to encoder set in the servo cylinder to control molten metal pressure.

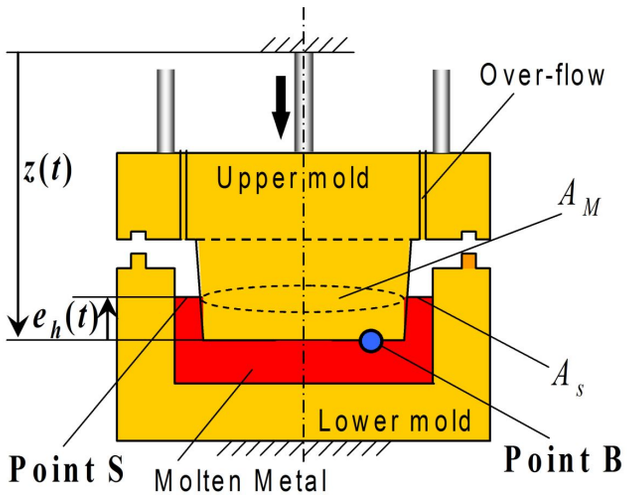

Figure 2. Diagrammatic illustration of pressing.

3. Modeling and Switching Control of Pressure

The online estimation of pressure inside the mold is necessary in the press casting system. The CFD analysis, based on the exact model of a Navier-Stokes equation, is very effective for analyzing fluid behavior offline and is useful for predicting the behavior and optimizing a casting plan. However, it is not sufficient for the design of a pressing velocity control or for the production of various mold shapes, because the exact model calculation would take too much time. Therefore, construction of a novel simple mathematical model for the control design in real time is needed in order to realize real-time pressure control. A simplified mold shape is shown in Fig. 3, where b_i and d_i are the height and the diameter, respectively. P_B is the pressure of the molten metal on a defect generation part where the pressure will cause a defect. The pressure fluctuation during pressing is approximated by a brief pressure model for an ideal fluid; i.e., an incompressible and viscous fluid is assumed. Here, $e_h(t)$ in Fig. 3 is the fluid level from under the surface of the upper mold. The head pressure of P_B is directly derived from $e_h(t)$. The press distance $z(t)$ of the upper mold is the distance that the upper mold must travel until it makes the bottom thickness of the product with the poured fluid in the lower mold. By increasing the pressing velocity or the flowing fluid velocity, the dynamical pressure changes rapidly by the effect of liquidity pressure. The hydrodynamic pressure for the peak fluid height is then involved in determining P_B. Therefore, P_B depends on the head and hydrodynamic pressure determined by using Bernoulli's theorem, and the pressure loss by viscosity flow friction is represented by the following equation:

$$P_b(t) = \rho g e_h(t) + \frac{\rho}{2}\left(1 + \lambda(T)\frac{l(e_h)}{d(e_h)}\right)\dot{e}_h(t)^2 \tag{1}$$

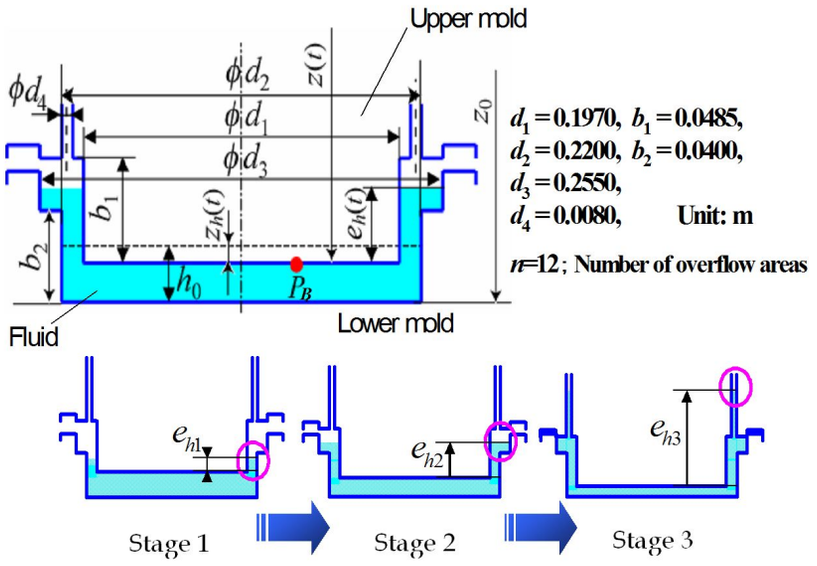

Figure 3. Mold shape and flow pass change.

where ρ[kg/m^3] is the density of fluid and g[m/s^2] is the acceleration of gravity. The adjustable parameter λ is the coefficient of the fluid friction depending on the fluid temperature, and $l(e_h)$ is the mold wall height of the part that causes shear stress in the vertical direction. The surface area of the flow channel decided by the mold shape is represented by $D_i(i$=1,2,3), and D_i changes as $D_1 = d_2 - d_1$; $D_2 = d_3 - d_1$; $D_1 = d_4/n$ during pressing. The number of overflow areas is represented by n. By the second term on the right-hand side in Eq. 1, the pressure P_B will rise rapidly due to the increasing fluid velocity when fluid flows into the overflow areas. The validity of the proposed pressure model as expressed by Eq. 1 was checked with several CFD simulations in our previous paper[7] under such the condition that temperature of molten metal is constant. The friction coefficient λ was then uniquely identified by a parameter identification fitting with the results derived from the CFD model. We have proposed a switching control for the pressing velocity to suppress the pressure increase. Thus, the pressing velocity necessary to suppress the pressure for defect-free production must be determined and implemented. Here, a multi-switching velocity pattern can be obtained using the following equation, and derived from the pressure model.

$$\dot{z}_k = \sqrt{\frac{2\left(P_{B\lim} - \rho g h_{uk}\right)}{\rho \max\left(A_{Sk}^2 / A_{Mk}^2\right)\left(1 + \lambda h_{uk} / D_k\right)}} \tag{2}$$

where the $k^{\text{th}}(k$ = 0,1,..)-step velocity is decided in order that the maximum velocity satisfies the desired pressure constraint P_{Blim}[Pa]. Because the diameter D_k and square ratio of surface

http://dx.doi.org/10.5772/51082

area $(A_{Sk}/A_{Mk})^2$ discontinuously change by each stage during pressing as shown in Fig. 3, a multi-switch velocity control is adopted. The number k of steps of pressing velocity with multi-switching can be determined by the mold shape in the case of Fig. 4, with the maximum value of k being 3. $\dot{z}_0$is the initial pressing velocity up until the point when the bottom surface of the upper mold contacts the top surface of the poured fluid. Derivation of Eq. 2 is straightforwardly calculated, and is omitted due to the paper space limitation.

When the pressing velocity changes from $\dot{z}_k$ to $\dot{z}_{k+1}$[m/s], the pressing distance z[m] is given by information of the mold shape and poured fluid volume. The design of the sequential velocity pattern such as the multi-switch point and each velocity must be adapted to particular mold shape. In the next pressing simulation, a switching velocity input is sequentially designed as shown in Fig. 4, where the press velocity pattern is formed as a trapezoidal shape by the switching position H_{uk} and the pressing acceleration a[m/s^2]. The control performance using the switching velocity of Eq. 2 designed by the proposed simple model was reasonably validated by CFD simulation as shown in Fig. 5. Although the flowing fluid has 3 flow pass stages during pressing for the mold shown in Fig. 3, the designed switching velocity pattern switches only 1 time. This is meant to set a maximum velocity of 50[mm/s] for $\dot{z}_1$at the 1st stage and$\dot{z}_2$at the 2nd stage to suppress extremely turbulent flow. $\dot{z}_3$at the 3rd stage of the narrow flow pass is then set to 6.9[mm/s]. Here the pressing acceleration is set to 1.5[m/s^2], and the total distance of pressing is 15[mm]. The molten metal properties in these simulations are shown in Table 1. The both pressure fluctuations as show in Fig.5 are satisfied under the pressure constraint value assumed as 10[kPa]. This pressure constraint value has been previously decided by using both the actual experimental test and the CFD analysis results of the press with several constant velocity patterns using molten metal.

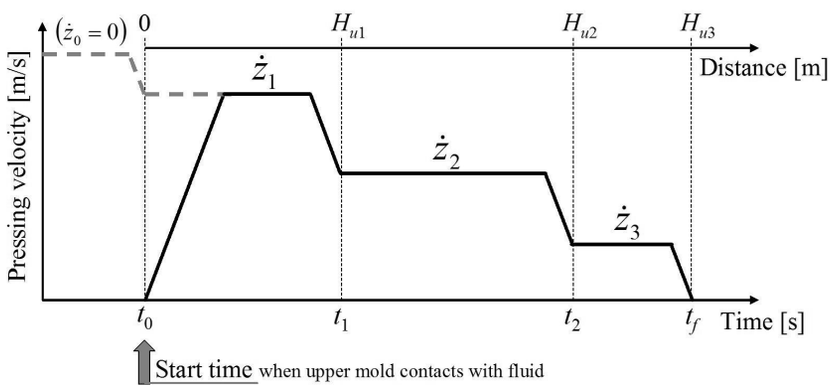

Figure 4. Pressing input shaped by trapezoidal velocities.

In the next chapter, parameter identification of λ [-] will be shown for each simulation condition to consider the pressure increase suppression for viscous fluid with a temperature decrease. Pressure has been rapidly increased while liquid flows into narrow pass $d(e_h)$[m] such that stage-3 in Fig. 3. As seen from Eq. 1, the effect of λ on the variation of pressure $P_b(t)$ becomes larger with the increase of liquid level e_h[m] and flow velocity $\dot{e}_h$ [m/s]. Thus,

exact value of $\lambda(T)$ must be given for the region of e_h and $\dot{e}_h$, because our purpose is to suppress the maximum pressure value. Therefore the fitting identification should be considered for only the flow during a short period in stage-3. Then, $T(t)$ is the lowest temperature during pressing because of the end time of pressing.

Density (const.)	7000 [kg/m^3]
Viscosity (T=1673)	0.02 [Pa•s]
Viscosity (T=1423)	0.2 [Pa•s]
Specific heat	771 [J/(kg•K)]
Thermal conductivity	29.93 [W/(m•K)]
Coefficient of heat transfer	1000 [W/(m^2•K)]
Liquidus temperature	1473 [K]
Surface tension coefficient	1.8 [-]
Contact angle	90 [deg]

Table 1. Molten metal properties.

4. Parameter Identification

Several parameter identifications of the fluid friction coefficient $\lambda(T_{end})$ at end time of pressing for various upper mold velocities have been carried out by comparing the proposed model with the CFD model analysis. The conditions of molten metal in these identification simulations are shown in Table 1. For the assumpution of temperature-drop cases, initial temperatures are set at 1673, 1623 and 1573[K] respectively. Although the

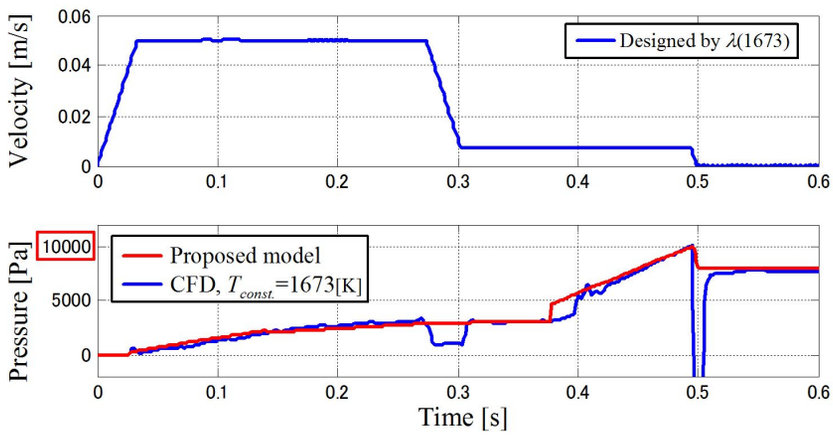

Figure 5. Pressure suppression ($T_{const.}$=1673[K]).

http://dx.doi.org/10.5772/51082

inverse trend of relative change between temperature-drop and viscosity-increase have been clarified, it seems difficult to obtain theoretical equation analytically on the relative change for a wide range of temperature variations and variety of materials. In the temperature drop from 1673 to 1423[K], the viscosity increase is arbitrarily assumed as the linearly dependence changing from 0.02 to 0.20[Pa•s]. Here, the maximum value of the pressure behavior by Eq. 1 of the proposed model is uniquly fitted to the results of the CFD model simuation.

In each case, the time-invariant parameter $\lambda(T_{end})$ have been identified as shown in Fig. 6. Using the designed velocity pattern in Fig. 5 conducted under the condition of constant temperature during pressing, the pressure behavior considering the fluid's heat flow to the molds exceeds the pressure constraint (top in Fig. 6) because of the higher viscosity(bottom in Fig. 6) as shown in Fig. 6. As seen from Fig. 6(a), (b) and (c), the lower temperature at end time induces the larger the value of λ. The temperature drop from start to end of pressing is almost 50[K] in these results. The pressure increase during pressing due to the larger value of $\lambda(T_{end})$ with the decreased temperature is confirmed. The simulation results of a simple model such that $\lambda(T_{end})$ is given as a constant value by fitting almost explains the results of the CFD model. Therefore, it is expected that we can conduct the control design using this simple pressure model under the restricted temperature change.

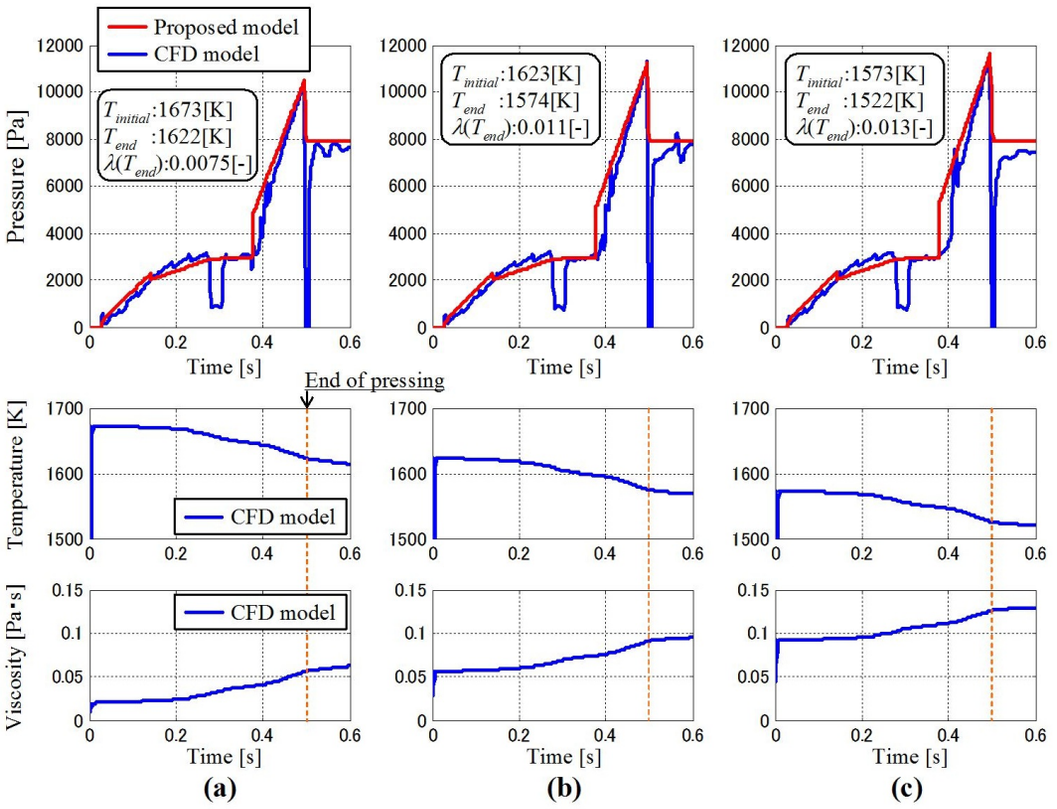

Figure 6. Parameter identification results.

5. Proposed Control Design and Results for Pressure Suppression

In this section, the proposed sequential switch velocity control considering the viscosity increase related to the temperature drop during pressing will be checked by using CFD model simulation with heat flow calculation.

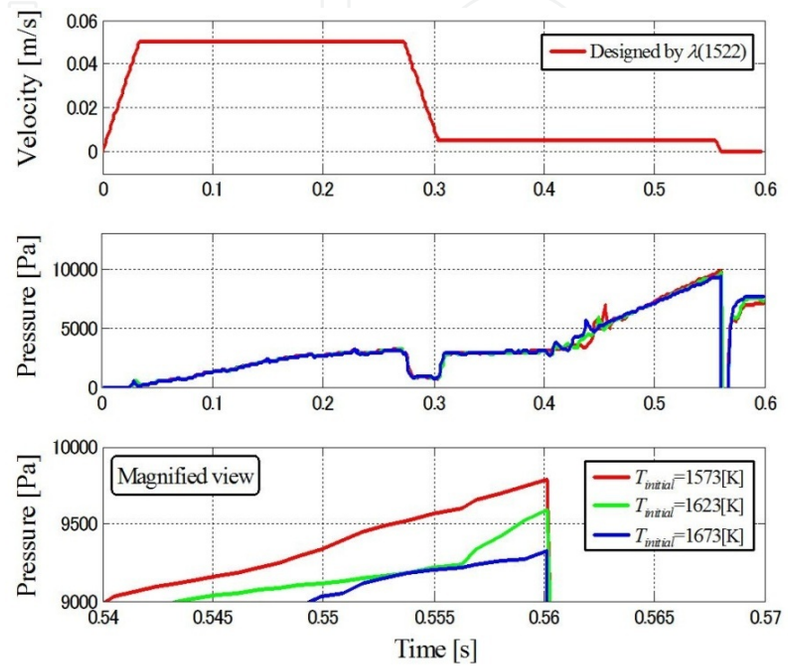

(a) case of optimum design

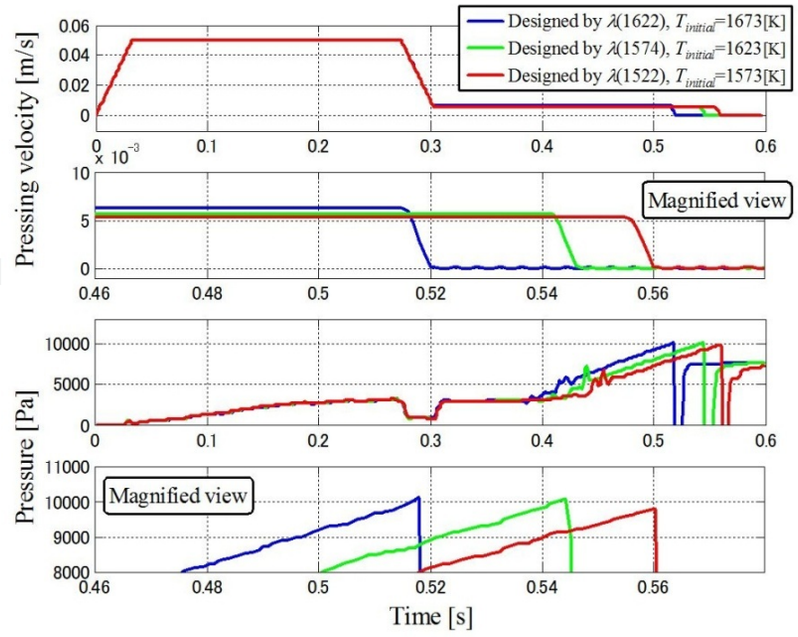

(b) case of robust design

Figure 7. Pressure suppression simulation using CFD simulator with designed velocities.

http://dx.doi.org/10.5772/51082

As example, for the designed pressing velocity patterns using $\lambda(T_{end})$ derived by the previous simulations, where T_{end} =1622, 1574 and 1522[K], the pressure suppression results for the each temperature condition of $T_{initial}$ =1673, 1623 and 1573[K] were checked for a upper pressure constraint: 10[kPa]. Here, the optimum design and robust design are introduced by using the proposed switching control method. Fig. 7(a, upper) shows a comparison of the designed velocity patterns and the magnified view. These lines show the desighed opitimum velosity patterns in the each case of temperature drop. The switched velocities (2nd constant velocity) are slightly different as 6.2, 5.5 and 5.2[mm/s], for the influence of the viscosity increase with the temperature drop. The end time of pressing are then 0.520, 0.546 and 0.560[s] respectively, and the biggest difference of the pressing time is only 0.040[s]. These velocity patterns which differs slightly, guarantees the exact suppression of pressure less than the constraint value as shown in Fig. 7(a, lower). Fig. 7(a, bottom) shows the magnified view of the pressure peak part at the end time of pressing. On the other hand, Fig. 7(b) shows pressure suppression varidation for a robust design of pressing velocity. The designed velocity by $\lambda(T_{end}$ =1522) in case of lowest temperature has been checked for $T_{initial}$ = 1673, 1623 and 1573[K]. As seen from Fig. 7(b, bottom), each muximum pressure value is suppressed under the upper constraint of pressure with some allowance. However, the end time is a little bit late compared with the optimum design case. As seen from this result, both methods satisfies the pressure suppression. However, optimum design satisfies both requirements of pressure constraint and shortening the operation time. On the other hand, robust design satisfies only pressure constraint, although this is useful, when temperature drop is not exactly known, but knows the least temperature for all batch operations. These analyses presented that the proposed control to suppress the maximum pressure of viscous flow with temperature drop can design the press switching velosity pattern optimally and robustly, for such the case that temperature drop from start time to end time of press is about 50[K].

6. Summary 1

In this section, we proposed an optimum control method of molten metal's pressure for a high-speed pressing process that limits pressure increase in casting mold. Influence of viscosity increase by temperature drop can be applied to the sequential pressing velocity design. The control design was conducted simply and theoretically, and included a novel mathematical model of molten metal's pressure considering viscous flow. The friction coefficient depending on temperature is meant to generate higher pressure than that in the case modeled without temperature drop during pressing. Using the pressure constraint and information on the mold shape, an optimum velocity design and robust velocity design using multi-switching velocity were derived respectively without trial-and- error adjustment. Finally, the obtained velocity reference's ability to control pressure fluctuation and to realize short cycle time was validated by the CFD simulations. In the near future, the proposed pressure model for optimizing the pressing process will be modified with the theoretical function models on temperature and viscosity-change, and futheremore real experiments will be done.

7. Experimental confirmation of physical metal penetration generation

In this section, we tried several molten metal experiments to clarify the mechanism of physical metal penetration growth and the boundary condition of physical metal penetration generation, and to validate the control performance of the feedforward method using the proposed pressing input design. Several experimental confirmations for the proposed pressure control method with a mathematical model of molten metal pressure were achieved for brake-drum production. The press casting productions with reasonable casting quality for each pressing temperature has been demonstrated through molten metal experiments.

7.1. Physical metal penetration and molten metal's pressure

Liquidus temperature of iron metal is about 1400[K], and the casting mould commonly used is heat-resistant green sand mould, for its advantages of high efficiencies of moulding and recycling. However, some defects are often caused by high pressurized molten metal [10]. Pressurized molten metal soaks into the sand mould surface, and then solidifies and form the physical metal penetration. Physical metal penetration as a typical defect related to higher pressurization inside the mould is offen ocurr on the casting surface. The metal penetration generated on complex shape product such as the products with tight, thin and multilayer walls, is difficult to be removed, while in the case of simple shape product, the defect can be removed by later surface processing. If the defect generation can be prohibited by pressing velocity adjustment, the sound iron castings can be obtained.

7.2. Mechanism of physical metal penetration

Physical factor caused metal penetration is explained by a diagrammatic illustration (Fig. 8) of interfacial surface between the molten metal and the sand mould, and a balance between two sides competing pressure on the boundary [11]. Fig. 8 also shows the relationship between the pressure balance and the metal penetration growth. In Fig. 8, on one side, the molten metal acts as a static pressure, P_{st} (Pa), a dynamic pressure, P_{dyn} (Pa), and a pressure, P_{exp} (Pa), because of expansion during solidification, which can force the liquid into the interstices of the sand grains. On the other side, due to the suppression effect of infiltration, the frictional loss pressure between the liquid metal and the sand grains, P_f (Pa), the pressure resulting from the expansion of the mould gasses, P_{gas} (Pa), and the pressure in the capillary, P_g (Pa), are all acted on the boundary surface. The governing equation that describes the pressure balance at the mould and metal interface can be written as:

$$P_g + P_f + P_{gas} = P_{st} + P_{dyn} + P_{\exp} \tag{3}$$

where the molten metal soaks into sand surface in the case that the right hand side of this equation is larger than the left hand side. As a result, the metal penetration defect is generated. Depending on the contact angle of iron and sand, the capillary pressure can be changed to be negative or positive as shown in Fig. 9. Thus, the pressure has both of beneficial or detrimental effects in preventing penetration at the same time. So capillary pressure can be neg-

ligible in Eq. (3). The P_{exp} can be eliminated in the case of the casting with open type mould as shown in Fig. 10. This means that P_{exp} is strongly related to the casting process design. Furthermore, using a slower filling velocity and selecting the moulding material that does not contain the component which can generate gasses, P_{dyn} and P_{gas} are then both negligible. Here, we obtain a simplified relational equation of pressure balance:

$$P_f = P_{st} \tag{4}$$

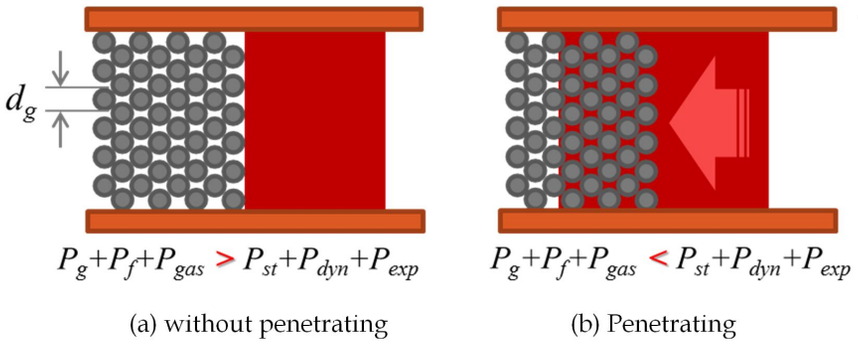

Figure 8. Pressure balance and penetration defect.

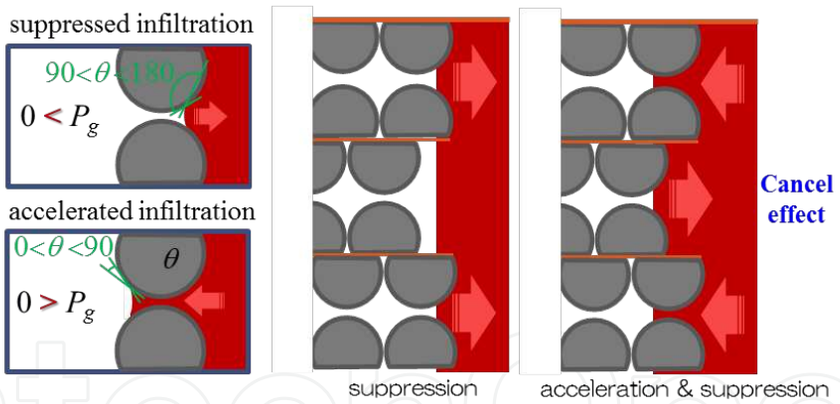

Figure 9. Cancel effect of capillary pressure.

7.3. Penetration phenomena under static pressure

In the conventional gravity casting, molten metal infiltrating into sand particles is generally generated when the high static pressure is added inside the mould. Sound casting products with metal penetration-free are designed such as whose maximum height of liquid head is under the allowable static pressure after filling. But, in the sand press casting case, it is confirmed that the penetration defect on the product surface is generated, even if the mould with a low static pressure is utilized. This indicates that the influences such as the dynamic pressure and the pressure due to the viscous friction depending on temperature drop, must be considered.

To observe the penetration growth under the force of gravity, a test experiment has been achieved with molten metal. A suggested casting mould shape and the casting are shown in Fig. 10. The molten metal was poured into the casting mould quickly at 1,400 ℃, and kept at 1673[K] until the end of filling. The casting mould is 1,000 mm in height and Φ45 mm in diameter. Here, the static pressure at the depth of H_l (m), P_{stb} is simply written as

$$P_{stb} = \rho g H_l \tag{5}$$

Where $\rho = 7{,}000$ (kg m^{-3}) is the density of molten metal, $g = 9.8$ (m s^{-2}) is gravity acceleration, H_l (m) is the vertical depth from the top of the casting product. Equation (5) can give the static pressure value easily, then a pressure constraint value for preventing the penetrated surface can be derived directly according to the maximum depth without metal penetration defect.

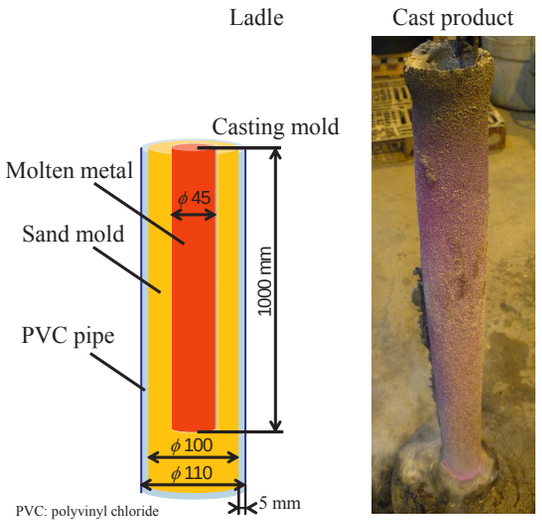

Figure 10. Gravity casting test with opened mold.

The mould release agent covering the casting pattern before moulding was not used in order to prevent the loss of the surface tension; the caking additive of the sand mould was selected for keeping steady the molten metal's properties. A cylindrical casting mold with the diameter of 45(mm) was selected for restricting the temperature distribution of molten metal during pouring. The elimination of physical factors for the penetration generation is considered as follows:

The surface of the product is observed by using the optical microscope. To investigate thoroughly under the casting surface, the cylindrical product is sliced along the direction perpendicularly to its axis, and the cut specimens at each depth, H_l, are pictured respectively. The penetration growths in the early phase and the final phase of solidification are confirmed clearly from Figs. 11(a) and (b). In Fig. 11(a) (H_l =150 (mm)), early phase of penetra-

http://dx.doi.org/10.5772/51082

tion in casting surface is identified, and some small sand grains are wrapped in cast metal. In the case of Fig. 11(b) (H_l = 950 (mm)) or bottom part of the product, the infiltration depth of molten metal to sand particles is over 1 (mm). Here, a high pressure loading about 65 (kPa) is estimated by calculating Eq. (5) of the static pressure. In the same way for H_l = 150 (mm), P_{bottom} is obtained as 10 (kPa). Therefore, molten metal's pressure, 10 (kPa), on the sand surface means an upper limit of penetration generation in this casting condition.

Metal penetration growths for each depth, H_l, with a 50 (mm) increment from 50 to 850 (mm) are shown in Fig. 12. Maximum infiltration depth observed in the investigation area of Fig. 12 is increased with vertical depth, H_l. The sand particles inside the metal cannot be removed easily by the next process such as the blast finishing and the grinding. Thus metal penetration defect must be prevented completely, and liquid pressure constraint 10 (kPa) in the case of H_l = 150 (mm) is set for defect-free production.

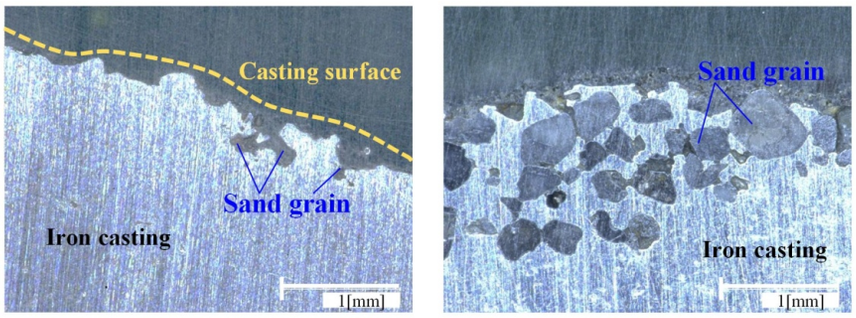

(a) *Hi* =150[mm] (b) *Hi* =950[mm]

Figure 11. Penetrated surface observation on casting skin.

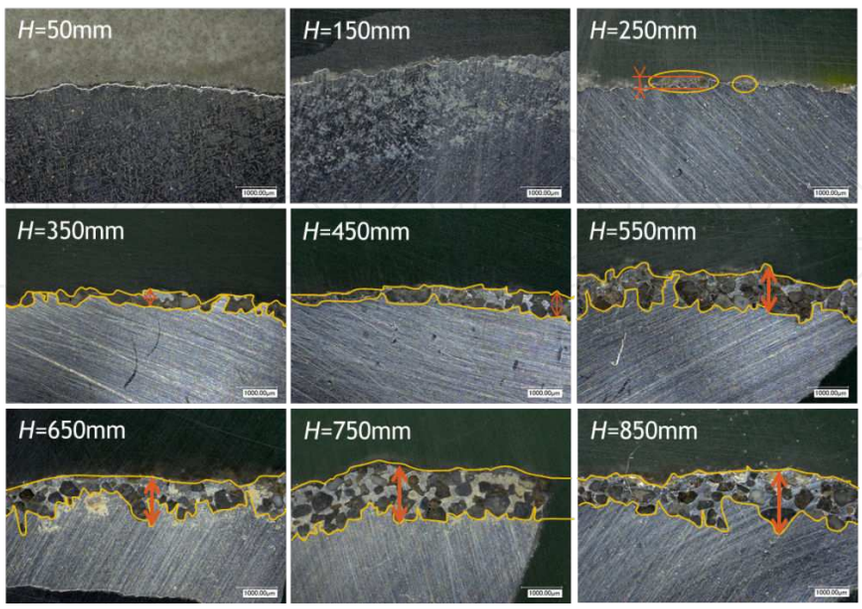

Figure 12. Metal penetration growths for each vertical depth.

7.4. Designed pressing velocity pattern

Substituting the obtained pressure constraint in the previous chapter and mould shape information of target cast product of the drum brake to Eq. (2) in previous chapter, the multi-step velocity pattern is sequentially calculated. Here, the pouring temperature is set to 1,400℃. The initial pressing velocity $\dot{z}_0$ until the upper mould contacts with top surface of poured molten metal, is the maximum pressing velocity, 375 (mm s^{-1}), of press machine. Each velocity for each flow situation are represented in Table 1. The vertical movement is driven accurately by servo cylinder and physical guide bars. The press casting equipment is shown in Fig. 13.

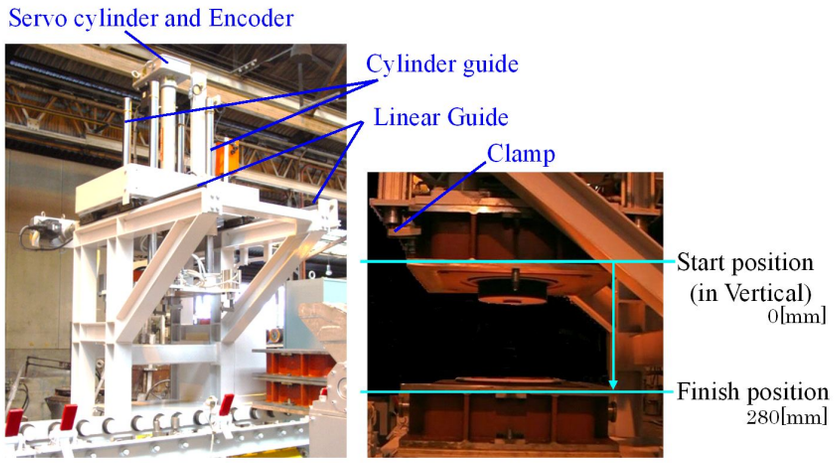

Figure 13. Press casting equipment and mold holding part.

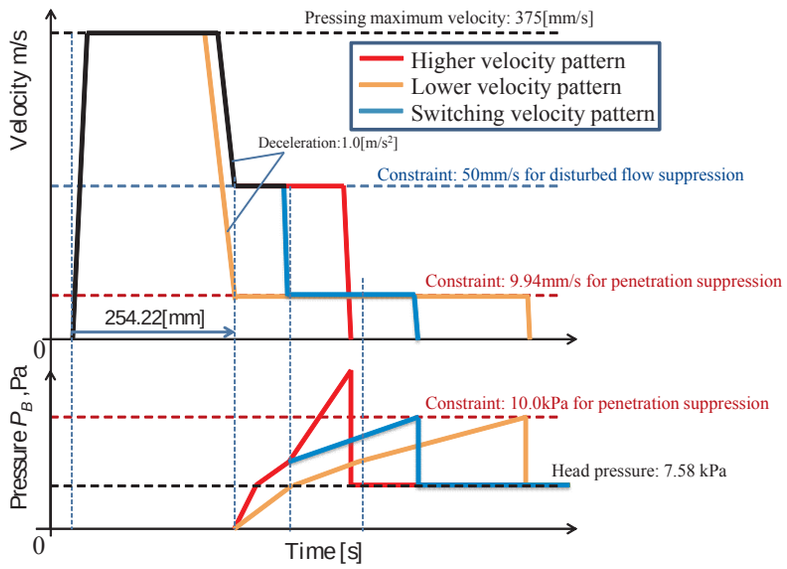

Figure 14. Designed pressing velocity patterns.

http://dx.doi.org/10.5772/51082

The multi-step velocity pattern is shown in Fig. 14. The acceleration of pressing movement is ideally assumed as constant 1 (m s^{-2}). The time constant of this drive system can be set to zero, because the identified exact value is 0.002 s or negligible. Therefore, step type velocity input is shaped as multi-overlapped trapezoid.

For discontinuous flow depended on mould shape, the pressing velocity, 50 (mm s^{-1}), was set in the case of wide liquid surface area. Here the first and second switching velocities, $\dot{z}_1$ and $\dot{z}_2$ calculated by considering the pressure constraint, are higher values in brackets of Table 2 This means that the pressing in the wide flow path must consider an upper limit velocity to prevent the disturbance flow causing overflow to the outside of mould. The velocity constraint was given by experimental trial and error process. Pressure suppression was evaluated by comparing with other conditions shown in Fig. 14.

	$\dot{z}_0$	$\dot{z}_1$	$\dot{z}_2$	$\dot{z}_3$	**Stop**
Pressing Velocity [mm/s]	375.00	50.00 (344.6)	50.00 (542.3)	9.94	0.00
Switching Position [mm]	0.00	254.22	254.22	279.44	280.20

Table 2. Multi-step velocities related to discontinuous change of flow passage.

7.5. Press casting experiments

Effectiveness of the pressure control with multi-step velocity design is confirmed by observing the casting surface. The surface roughness of tested specimens under the given conditions is shown in Fig. 15. In the case of higher velocity pressing (HV: $\dot{z}_1 = \dot{z}_2 = \dot{z}_3$ =50.00[mm/s]), the product surface is the roughest. Dash line circles on the surface show the infiltrated sand particles. This result indicates that the metal penetration defect is clearly generated by pressing with high pressure over 10 kPa. Both in the case of lower velocity (LV: $\dot{z}_1 = \dot{z}_2 = \dot{z}_3$ =9.94[mm/s]) and proposed switching velocity (SV: $\dot{z}_1 = \dot{z}_2$ =50.00[mm/s], $\dot{z}_3$ =9.94[mm/s]), sound products of smoothed surface or defect-free production can be obtained. The pictures of magnified product surface in Figs. 15(a) to (c) are given under the experimental condition of higher pressing temperature 1,400℃ (HT). Here the pressing temperature is adjusted by monitoring with a sensor and naturally cooling the molten metal with the pouring temperature, about 20~30 degrees higher than the pressing temperature. Fig. 15 show that the different surface state does not depend on temperature.

Fig. 16 shows the overview of the casting pressed by the switching velocity pattern (SV). From these photos, better product of SV-HT is clearly verified, because the switch velocity is designed just for the higher temperature 1,400℃. There is a tiny penetration in casting of SV-LT. Higher pressure at the same pressing is generated with higher viscous flow related to lower temperature.

Consequently, the proposed pressing pattern shows defect-free production in the short filling time as almost same as the highest pressing pattern considered with the disturbance flow sup-

pression. The time difference between the cases of HV-LT and SV-LT is only 0.07 (s). This result shows 2 (s) shorter than the case of LV-LT with well production. Furthermore, the comparative validation of the different temperature in Fig. 16 shows that the pressing velocity is designed properly for the monitored poured liquid temperature immediately before pressing. The proposed press casting production considering molten metal's pressure suppression will meet the requirement for practical use with temperature variation range.

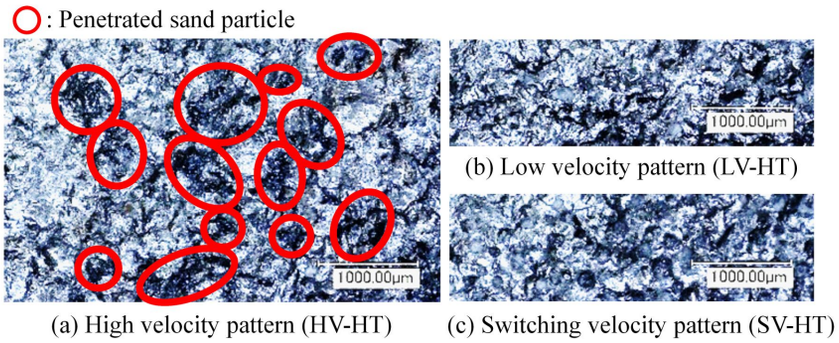

Figure 15. Product surface observations for penetration defect.

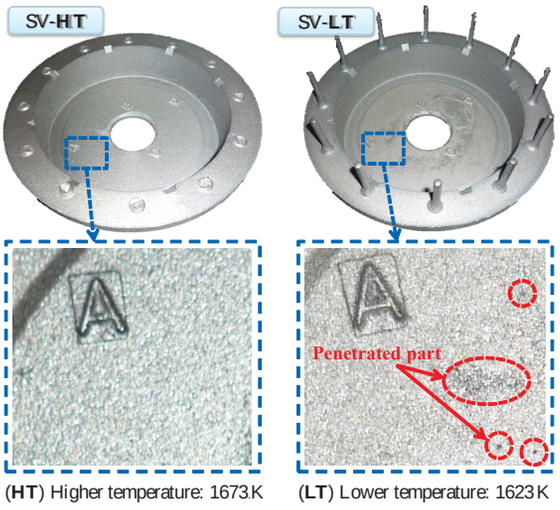

Figure 16. Casting product in case of different temperature conditions.

7.6. Summary 2

The pressing velocity control was proposed in order to suppress increasing pressure with short filling time. A pressure limitation of the penetration generation has been confirmed by a gravity casting experiment for a relation analysis between the static (head) pressure and

the infiltrated metal length. Next, by applying the obtained constraint pressure for defect-free to the theoretical control design method with pressing velocity adjustment, the effectiveness of the proposed control method is validated by molten metal experiment. The final results showed that the proposed pressing control realizes sound cast production in almost the same filling time with the high speed pressing, which can cause defect. These confirmation results indicate that the press casting process with our proposed control technique can be adapted properly for environment change such as temperature drop in continual process.

8. Modelling and Control Unstationary Flow

The online estimation of pressure inside the mold is necessary in the press casting system. The CFD analysis, based on the exact model of a Navier-Stokes equation, is very effective for analyzing fluid behavior offline and is useful for predicting the behavior and optimizing of a casting plan [8-9]. However, it is not sufficient for the design of a pressing velocity control or for the production of various mold shapes, because the exact model calculation would take too much time. Therefore, construction of a novel simple mathematical model for the control design in real time is needed in order to realize real-time pressure control.

To analyze flowing liquid motion during pressing, several experiments with colored water and an acrylic mold have been carried out as shown in Fig. 17. The nature of flow will dictate the rectangular Cartesian, cylindrical and spherical coordinates etc. In 3D flow, velocity components exist and change in all three dimensions, and are very complicated to study. In the majority of engineering problems, it may be sufficient to consider 2D flows. Therefore the acrylic mold shaped flat is prepared for flow observation of liquid. The main purpose of our study on the press casting process is to suppress the defect generation of casting product. Air Entrainment during filling is one of the most important problems to solve for flow behavior by adjustment of pressing velocity. If the air is included in molten metal, it will stay and be the porosity defect. By the past experimental result, upper mold velocity less than 50 mm s^{-1} of pressing without air entrainment has been confirmed. From this fact, the pressure model construction is considered for only stationary flow in vertical without air entrainment, or the pressing velocity lower than the upper limit for the defect-free for air porosity.

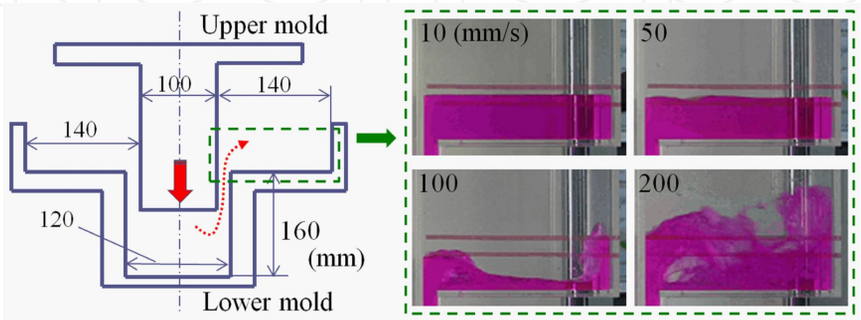

Figure 17. Observational experiment of unstationary flow.

8.1. Pressure Model of Unstationary Flow

Fig. 18 shows the rising flow during pressing and each stream line of molten metal's flow. The unstationary Bernoulli equation for two points: S and B on a given stream line in the flow of an incompressible fluid in the presence of gravity is

$$\int_B^S \frac{\partial U}{\partial t} ds + \frac{1}{2} U_S^2 + \frac{P_S}{\rho} + g e_S = \frac{1}{2} U_B^2 + \frac{P_B}{\rho} + g e_B, \tag{6}$$

where ρ kg m^{-3} is the density of fluid and g m s^{-2} is the acceleration of gravity. The integral is taken along the stream line, and cannot be easily evaluated in general. For the rising flow in press casting, the integral can be quite closely approximated by an integral along the vertical axis. In the case of Fig. 18, the stream line is taken to vertically extend from the bottom surface of upper mold to the free surface of fluid. Placing the origin to the bottom of upper mold surface, substituting $P_S = 0$ (based on gauge pressure) and $e_h = e_S - e_B$, and neglecting $\dot{e}_B^2$ as $\dot{e}_S^2 \dot{e}_B^2$, then the Eq. (6) simplifies to

$$P_B = \rho \left(\ddot{e}_h e_h + \frac{1}{2} \dot{e}_h^2 + g e_h \right) \tag{7}$$

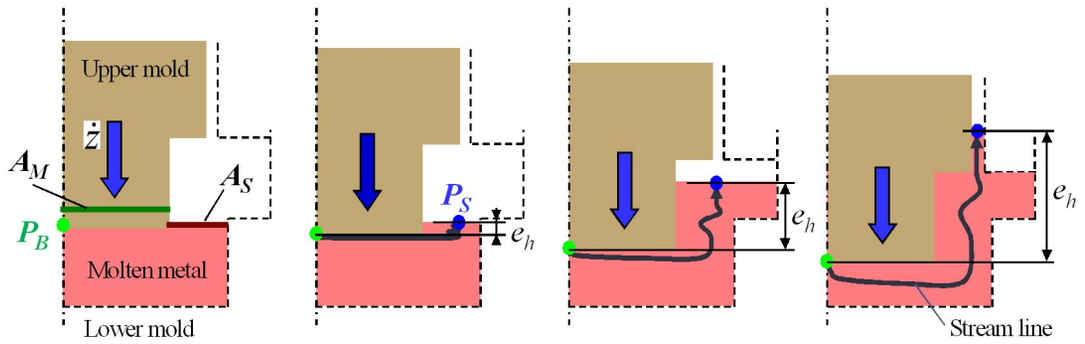

Figure 18. Change of stream line of rising liquid.

The fluid velocity $\dot{e}_h$ m s^{-1} at the free surface A_S m^2 relates the mold surface area A_M m^2 at the same height with the free surface and the pressing velocity $\dot{z}$ m s^{-1} as shown in Fig. 18.

Here, rewriting the extended Bernoulli equation in terms of z m and considering with the initial volume of fluid poured in the lower mold, one obtains

$$P_B = \rho \frac{A_M^2(e_h)}{A_S^2(e_h)} \left(\ddot{z} z + \frac{1}{2} \dot{z}^2 \right) + \rho g f(V_p, z) + \Delta p(T, e_h) \tag{8}$$

http://dx.doi.org/10.5772/51082

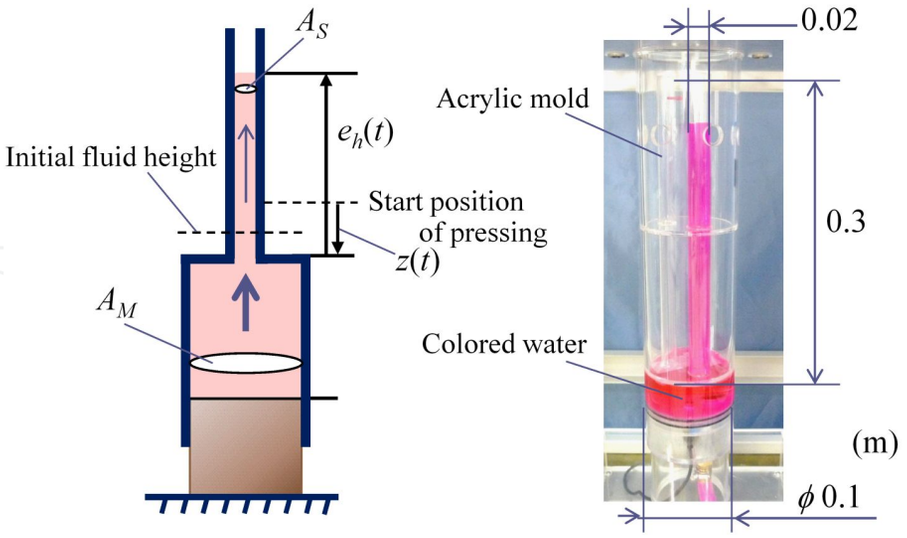

Figure 19. Mold shape for a part of overflow.

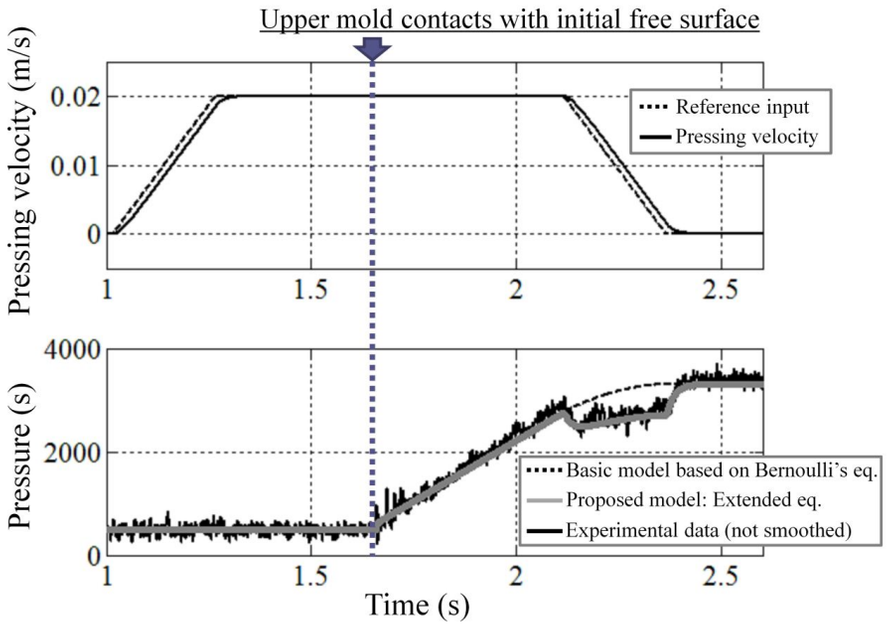

Figure 20. Comparative result between proposed mathematical model and measured pressures.

where $\Delta p(T, e_h)$ means a pressure loss depended on liquid temperature change on flow from upstream to downstream and the vertical flow length e_h contacting with the wall.

To confirm the proposed pressure model for pressed liquid, several experiments using simplified shape mold and water have been carried out. The acrylic mold and its shape are shown in Fig. 19. The vertical movement of the upper mold is derived accurately for reference input of velocity curve by servo-press system. In the experiment as shown in Fig. 20,

the actual pressing velocity (solid line) is reshaped for reference input (dashed line). This slight difference is due to the driving motor characteristic approximated by first order lag element with the time constant: 0.020 s. As an example of the confirmation result with proposed model, pressure behavior measured by piezoelectric-type pressure sensor (AP-10S, by KEYENCE Corp.) is shown in Fig. 20 (lower), solid line. Here, the maximum pressing velocity is set to 20 mm s^{-1}, and total moving displacement of press is 22 mm. The dashed line in Fig. 20 (lower) is the pressure calculated result with Bernoulli's equation for steadyfluid flow as described. As seen from this figure, the calculated result of the proposed pressure model considering the unstationary flow, is in excellent agreement with actual pressure behavior during pressing.

8.2. Viscous Influence

In a practical situation, the temperature decrease due to the heat transfer between the molten metal and the mold surface should be considered as an important influence on liquid pressure during pressing. For decreasing temperature, the viscosity increase and higher pressure are then generated, and therefore the penetration defect occurs. Generating the shearing force on the wall surface of the flow path, a point at the upstream is pressurized higher than one at the downstream. Considering the pressure difference between P_B at the bottom of the upper mold and P_S at the free surface, it is written as $\Delta p = P_B - P_S$. Here, the equilibrium relation of force between the shearing force F_w and Δp is derived as following equation by considering the frictional loss pressure.

$$F_w = \frac{\pi}{4}(d)^2 \Delta p = \pi d l \tau \tag{9}$$

Here, using the friction coefficient λ depended on molten metal's temperature T (K), Δp Pa can be represented by the following equation:

$$\Delta p(T, e_h) = \rho \frac{A_M^2(e_h)}{A_S^2(e_h)} \frac{\lambda(T) l(e_h)}{2d(e_h)} \dot{z}^2 \tag{10}$$

After substituting Eq. (10) to Eq. (9), the proposed pressure model conformable to the complex model of CFD is constructed by depending on liquid temperature to express more precisely the molten metal's pressure. Here, $\lambda(T)$ means the coefficient of fluid friction depending on the fluid temperature; it will be sole unknown parameter of the proposed model. $l(e_h)$ is the mold wall length of the part that causes shear stress in the vertical direction. $D_i (i = 1, 2, 3)$ represents the surface area of the flow channel decided by the mold shape as shown in Fig. 3, and D_i will change as $D_1 = d_2\text{-}d_1$, $D_2 = d_3\text{-}d_1$, $D_1 = d_4/n$ during pressing. n is the number of overflow areas. By the pressing velocity term in the newly proposed pressure model, it is easily understood that P_B will be rapidly rising due to the increasing fluid velocity when fluid flows into narrow flow path areas.

8.3. Optimized pressure control with continuous velocity input of pressing / Summary 3

In this section, a mathematical modeling and a switching control for pressure suppression of pressurized molten metal were discussed for defect-free production using the press casting. For the complex liquid flow inside vertical path during pressing, the liquid's pressure model for the control design was newly proposed via the unstationary Bernoulli equation, and was represented in excellent agreement with actual pressure behavior measured by a piezoelectric-type pressure sensor. Next, the sequential pressing control design with switching velocity for the high-speed pressing process that limits pressure increase, was applied with considering the influence of viscous change by temperature drop. Using the pressure constraint and information on the mold shape, an optimum velocity design and robust velocity design were derived respectively without trial-and-error adjustment. Consequently, the effectiveness of the pressing control with reasonable pressure suppression has been demonstrated through the CFD. In the near future, the proposed pressure model for optimizing the pressing process will be modified with the theoretical function models on temperature and viscosity-change, and furthermore real experiments with molten metal will be done.

Author details

Ryosuke Tasaki[1*], Yoshiyuki Noda[2], Kunihiro Hashimoto[3] and Kazuhiko Terashima[1]

*Address all correspondence to: tasaki@syscon.pse.tut.ac.jp

1 Department of mechanical engineering, Toyohashi university of Technology, Japan

2 Department of mechanical system engineering, Yamanashi University, Kohu-city, Japan

3 Sintokogio, Ltd., Japan

References

[1] Terashima, K., Noda, Y., Kaneto, K., Ota, K., Hashimoto, K., Iwasaki, J., Hagata, Y., Suzuki, M., & Suzuki, Y. (2009). Novel creation and control of sand mold press casting "post-filled formed casting process. *Foundry Trade Journal International (The Journal of The Institute of Cast Metals Engineers)*, 183(3670), 314-318.

[2] Terashima, K., Noda, Y., Kaneto, K., Ota, K., Hashimoto, K., Iwasaki, J., Hagata, Y., Suzuki, M., & Suzuki, Y. (2009). Novel creation and control of san mold press casting "post-filled formed casting process". *Hommes & Fonderie*, 396(396), 17-27.

[3] Noda, Y., & Terashima, K. (2007). Modeling and feedforward flow rate control of automatic pouring system with real ladle. *Journal of Robotics and Mechatronics*, 19(2), 205-211.

[4] Noda, Y., Yamamoto, K., & Terashima, K. (2008). Pouring control with prediction of filling weight in tilting-ladle-type automatic pouring system. *International Journal of Cast Metals Research, Science and Engineering of Cast Metals, Solidification and Casting Processes, AFC-10 Special*, 21(1-4), 287-292.

[5] Hu, J. V. J. H. (1994). Dynamic modeling and control of packing pressure in injection molding. *Journal of Engineering Materials and Technology*, 116(2), 244-249.

[6] Tasaki, R., Noda, Y., & Terashima, K. (2008). Sequence control of pressing velocity for pressure in press casting process using greensand mould. *International Journal of Cast Metals Research, Science and Engineering of Cast Metals, Solidification and Casting Processes, AFC-10 Special*, 21(1-4), 269-274.

[7] Tasaki, R., Noda, Y., Terashima, K., & Hashimoto, K. (2009). Pressing velocity control considering liquid temperature change in press casting process. *Proc. of IFAC Workshop on Automation in Mining, Mineral and Metal Processing*, 65.